A Sensitive Electrochemiluminescence Immunosensor for Celiac Disease Diagnosis Based on Nanoelectrode Ensembles

Henok B. Habtamu,[†,‡] Milica Sentic,[‡,§] Morena Silvestrini,[†] Luigina De Leo,[∥] Tarcisio Not,[∥,⊥] Stephane Arbault,[‡] Dragan Manojlovic,[§] Neso Sojic,[*,‡] and Paolo Ugo[*,†]

[†]Department of Molecular Sciences and Nanosystems, University Ca'Foscari of Venice, via Torino 155, 30172 Venezia Mestre, Italy
[‡]Institut des Sciences Moléculaires, CNRS UMR 5255, University of Bordeaux, ENSCBP, 33607 Pessac, France
[§]Faculty of Chemistry, University of Belgrade, 11000 Belgrade, Serbia
[∥]Institute for Maternal and Child Health - IRCCS "Burlo Garofolo", 34100 Trieste, Italy
[⊥]University of Trieste, 34127 Trieste, Italy

Supporting Information

ABSTRACT: We report here the design of a novel immunosensor and its application for celiac disease diagnosis, based on an electrogenerated chemiluminescence (ECL) readout, using membrane-templated gold nanoelectrode ensembles (NEEs) as a detection platform. An original sensing strategy is presented by segregating spatially the initial electrochemical reaction and the location of the immobilized biomolecules where ECL is finally emitted. The recognition scaffold is the following: tissue transglutaminase (tTG) is immobilized as a capturing agent on the polycarbonate (PC) surface of the track-etched templating membrane. It captures the target tissue transglutaminase antibody (anti-tTG), and finally allows the immobilization of a streptavidin-modified ruthenium-based ECL label via reaction with a suitable biotinylated secondary antibody. The application of an oxidizing potential in a tri-*n*-propylamine (TPrA) solution generates an intense and sharp ECL signal, suitable for analytical purposes. Voltammetric and ECL analyses evidenced that the ruthenium complex is not oxidized directly at the surface of the nanoelectrodes; instead ECL is generated following the TPrA oxidation, which produces the $TPrA^{\bullet+}$ and $TPrA^{\bullet}$ radicals. With NEEs operating under total overlap diffusion conditions, high local fluxes of these reactive radicals are produced by the nanoelectrodes in the immediate vicinity of the ECL labels, so that they efficiently generate the ECL signal. The radicals can diffuse over short distances and react with the $Ru(bpy)_3^{2+}$ label. In addition, the ECL emission is obtained by applying a potential of 0.88 V versus Ag/AgCl, which is about 0.3 V lower than when ECL is initiated by the electrochemical oxidation of $Ru(bpy)_3^{2+}$. The immunosensor provides ECL signals which scale with anti-tTG concentration with a linearity range between 1.5 ng·mL^{-1} and 10 μg·mL^{-1} and a detection limit of 0.5 ng·mL^{-1}. The sensor is finally applied to the analysis of anti-tTG in human serum samples, showing to be suitable to discriminate between healthy and celiac patients.

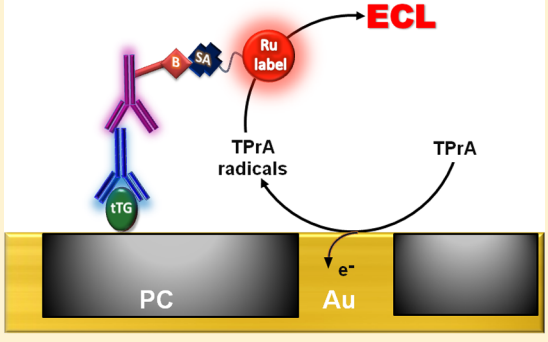

Celiac disease (CD) is a gluten-dependent autoimmune disorder with a prevalence of 1% in the general population,[1,2] 1.5% in children, and 2.7% in the elderly.[3−5] The clinical conditions of CD vary from mild to severe, and some patients can be asymptomatic for years. When there is a later diagnosis of CD, there is a greater likelihood of serious illness and excess mortality.[6] Early diagnosis and treatment with a gluten-free diet reduces mortality and the prevalence of CD-associated disorders. Although definitive diagnosis of CD is still based on histological changes in small intestinal mucosa, whose detection requires biopsy, serological tests for CD screening based on detection of antitransglutaminase type-2 antibodies (anti-tTG) are less invasive.[7] Given the high prevalence of CD and the implications of a late detection, several simple, cheap, and rapid immunoassays were developed as a first step toward speeding up CD diagnosis in the physician's office.[8,9] Of interest, these rapid tests might greatly help the physician to make a preliminary diagnosis of CD in resource-constrained countries where diarrheal disease and malnutrition are common.[10,11] Anti-tTG immunoglobulins are classified into two isotypes, namely, IgA and IgG type. Immunoglobulin A (anti-tTG IgA) is the isotype typically determined as target analyte for serological CD screening.[12,13] However, IgA-deficient CD patients are not identified by this analysis.[14] Moreover, focusing on CD diagnosis in very young children for whom biopsy is not an eligible test, it has been found that only 87% of CD patients younger than 2 years of age showed high serum levels of IgA anti-tTG vs 96% for celiac children older

Accepted: November 10, 2015

than 2 years.[15,16] On the other hand, serological diagnosis based on IgG assays at present does not look as a valid alternative for general screening because IgG-based assays have significantly poorer clinical sensitivity and specificity than IgA-based analysis.[12] From this basis, it is evident that the development of a IgG-based diagnostic method with improved sensitivity and specificity is highly required. Many trials have been made to develop a variety of electrochemical methods,[17−22] but, so far, no unique confirmatory serological method has been adopted for practical use. Accordingly, we propose herein a novel anti-tTG immunosensor utilizing an original electrogenerated chemiluminescence (ECL) detection strategy based on nanoelectrode ensembles (NEEs).

ECL is the phenomenon of light emission produced by the excited state of a luminophore which results from an initial electrochemical reaction.[23,24] This luminescence process has attracted enormous attention in bioanalysis owing to its inherent analytical performances. Indeed, because no excitation light source is required to induce ECL, the background signal is extremely low, and thus, the technique is highly sensitive at physiological pH with low detection limits.[24−27] Moreover, ECL provides additional advantages such as wide linear dynamic range, selectivity, and stability of the luminophore. In addition, it is relatively easy to conjugate the luminescent species to biomolecules such as antibodies, DNA, or RNA.[28−33] Therefore, the luminophore is classically used as an ECL label in bioassays.[34,35] The model system involving $Ru(bpy)_3^{2+}$ as the light-emitting species and tri-*n*-propylamine (TPrA) as the coreactant forms the basis of a large number of commercially available bead-based ECL immunoassays, such as for cardiac and infectious diseases, thyroid disorders, and as tumor markers.[24,26,36] The excellent sensitivity of such immunoassays is due to the fact that ruthenium centers located at micrometric distances from the electrode generate ECL.[37−39] Indeed, in this case, only the coreactant TPrA is oxidized at the electrode, and the resulting radicals, $TPrA^{\bullet+}$ and $TPrA^{\bullet}$, diffuse over short distances and react with the luminophore to generate its excited state.[39] So this mechanistic path does not require the direct oxidation of $Ru(bpy)_3^{2+}$ at the electrode surface to generate *in fine* the ECL emission. In addition, it occurs at a potential ~300 mV lower than for the routes involving the $Ru(bpy)_3^{2+}$ oxidation.

NEEs are random arrays of nanoscopic electrodes typically prepared by the electroless deposition of gold within the nanopores of track-etched polycarbonate (PC) membranes.[40−43] The nature of the faradaic current depends on the distance between the nanodisks, on the solution viscosity, and on the time scale of the experiment.[44−46] When commercial track-etched membranes are used, the obtained NEEs operate in the total overlap diffusion regime,[40,47] which means that electroctive species diffuse via semi-infinite planar diffusion with respect to all the surface of the NEE (i.e., nanoelectrodes and insulator between them). Recently, the properties of NEEs have been exploited to develop electrochemical biosensors[48] in which relatively high amounts of bioreceptor molecules were immobilized directly on the PC of the NEEs. The integration between the biorecognition event and the electrochemical acquisition of the signal is ensured by the presence in the electrolytic solution of redox mediators; these can diffuse all over the geometric area of the NEE and shuttle electrons to redox labels bound to the biorecogniton layer. This approach has been applied to develop sensitive affinity biosensors suitable to detect the human epidermal growth factor receptor HER2 overexpressed in breast-cancer cells,[49] DNA sequences for virus genotyping,[50,51] ligand proteins of interest for cultural heritage diagnostics,[52] and enzyme-based glucose sensing.[53]

In the present work, we combine for the first time the remarkable properties of NEEs with the excellent detection capability of ECL in order to develop a novel sensing method based on anti-tTG IgG determination, for CD diagnosis in human serum. A major originality of the current approach is to separate physically the location of the initial electrochemical reaction at the Au NEEs (i.e., oxidation of the coreactant) from the ECL-emitting region where the luminophore label is immobilized on the PC substrate. To this aim, the capturing agent tTG is at first bound onto the PC of a NEE so that, when incubated with the sample, it reacts with the target analyte, namely, anti-tTG IgG antibody (Scheme 1). The biorecognition chain is continued by coupling the captured anti-tTG antibody with a biotinylated secondary anti-IgG antibody. A streptavidin $Ru(bpy)_3^{2+}$ derivative (SA-Ru) is then used as the ECL label, which binds to the PC surface only in case of positive analytical response. Finally, the ECL emission is generated by applying a suitable electrochemical potential in a phosphate buffer solution (PBS) containing the sacrificial TPrA coreactant. Thanks to the customized architecture of the platform, the TPrA coreactant is oxidized at the nanoelectrodes, and the resulting radicals diffuse all over the geometric area of the NEEs to reach the $Ru(bpy)_3^{2+}$ label on the PC to produce ECL. With NEEs, the first advantage is that high local fluxes of reactive radicals are generated due to the nanosize of the electrode. The second one is that they are produced in the immediate vicinity of the ECL labels, which are immobilized on the PC, so that they can efficiently generate the ECL signal. Finally, they offer the opportunity to miniaturize such an analytical platform.

Scheme 1. Scheme Showing the Design of the Immunosensor (Not in Scale)[a]

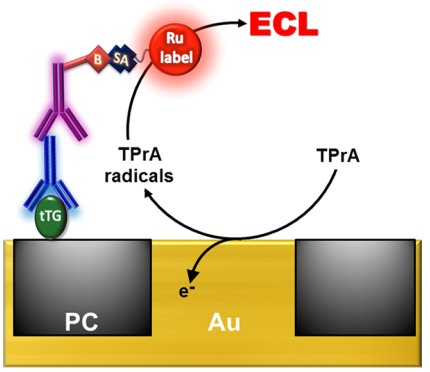

[a]The PC surface is first modified with the capture protein, tTG. The assay is performed by incubating it with a sample containing the target (i.e. anti-tTG antibody) and then in a solution of a biotinylated secondary antibody. The final step consists in attaching the ECL label by exposing the immunosensor to a solution containing a streptavidin-modified $Ru(bpy)_3^{2+}$ complex (SA-Ru). Oxidation of TPrA occurs at each Au nanoelectrode of the NEEs, and the resulting radicals, $TPrA^{\bullet+}$ and $TPrA^{\bullet}$, diffuse over short distances and react with the luminophore label attached to the PC to generate the ECL emission.

EXPERIMENTAL SECTION

Materials. An Autolab PGSTAT30 potentiostat, a Hamamatsu photomultiplier tube (PMT) equipped with KEITHLEY 6485 picoammeter, and a high-voltage power supply Hamamatsu Photonics model C9525 were used for electrochemical and ECL experiments. SEM images were obtained with a Jeol JSM-6700F field-emission scanning electron microscope (FE-SEM). All electrochemical and ECL experiments were performed using an Ag/AgCl/3 M KCl reference electrode and a platinum wire as counter electrode.

Bis(2,2′-bipyridine)-4′-methyl-4-carboxybipyridine-ruthenium *N*-succinimidyl ester bis(hexa-fluorophosphate) and streptavidin from *Streptomyces avidinii*, Tween 20, bovine serum albumin (BSA), and biotinylated goat antihuman secondary antibody were purchased from Sigma. Tissue transglutaminase (tTG) was prepared as previously described.[1] Monoclonal mouse anti-tTG (CUB 7402) was purchased from BioOptica and biotinylated goat antimouse secondary antibody from Dako. Serum samples were obtained from five biopsy proven celiac children tested positive only for anti-tTG IgA (9777, 9782, 9784, 9809, 9830) and from two children without autoimmunity and gastrointestinal disorders, tested negative for anti-tTG both IgA and IgG (9463, 9597). All patients were diagnosed at the Pediatric Hospital "Burlo Garofolo" (Trieste, Italy). Gold electroless plating solution (Oromerse Part B, Technic Inc.) and hydrophilic track-etched PC filter membranes (SPI-pore, membrane diameter: 47 mm, thickness: 6 μm, nominal pore diameter: 30 nm, pore density: 6×10^8 pores/cm^2) were used for manufacturing NEEs. All other reagents were of analytical grade.

Methods. *Modification of Streptavidin with Ru(bpy)$_3^{2+}$ Complex (SA-Ru).* The modification was done as reported with some modifications.[31] Briefly, 1 mg of streptavidin was dissolved in 1 mL of Milli-Q water. Then 100 μL of this solution was added to 810 μL of water and 90 μL of 1× PBS pH 7.4 and mixed with 1 mg of Bis(2,2′-bipyridine)-4′-methyl-4-carboxybipyridine-ruthenium *N*-succinimidyl esterbis(hexa-fluorophosphate), which was dissolved in 100 μL of dried DMSO. The mixture was kept at 4 °C with continuous stirring for 4 h. Then it was purified by dialysis in PBS (1×) using Slide-A-Lyzer Dialysis Cassettes 10k molecular weight cutoff from Thermo Scientific for about 16 h. The Ru-SA complex was stored at +4 °C until used.

Fabrication of the NEEs. The Au NEEs were prepared by electroless deposition of gold in track-etched PC filter membranes using an already published procedure[40] and following updates.[54,55] During the electroless deposition of gold from a solution, the pores of the PC membrane were filled with individual metal nanowires whose heads are exposed to the electrolyte solution so that the surface of the NEE is composed of millions of randomly spaced gold nanodisks. The membrane bearing the nanodisks was assembled into electrodes of suitable geometry and size as previously described[47] (see Supporting Information for details).

Preparation of the Immunoassay and Analytical Protocol. An aliquot of 10 μL of 10 μg·mL^{-1} tTG solution in 0.1 M carbonate buffer (pH 9.2) was dropped on the NEE and incubated for 2 h at 25 °C. It has been previously shown[49,52] that, under these conditions, antigen and antibody proteins bind preferentially on the PC of NEEs. The tTG-NEE was subsequently blocked with 1% BSA for 30 min followed by incubation with 10 μL standard solution of anti-tTG or serum sample in 1× PBS pH 7.4 for 60 min. After washing with 1× PBS (pH 7.4) containing 0.05% Tween 20, the captured primary antibody was coupled with biotinylated Goat antimouse or antihuman IgG secondary antibody for 60 min. It was further incubated for 30 min at +4 °C with the SA-Ru solution. In all the procedures, wet filter paper was put in the incubation container and sealed to avoid evaporation of the solution; incubations were made at 25 °C except the last step, and all incubations were followed by thorough rinsing with buffer solution. Finally, the biosensor was dipped in a three-electrode electrochemical cell containing 0.1 M TPrA in 0.1 M PBS (pH 7.4) previously deaerated with nitrogen for 20 min. ECL and cyclic voltammograms were recorded concurrently at a scan rate of 100 mV/s. The ECL intensity was measured using a PMT at a bias voltage of −750 V.

Fluoroenzyme immunoassay for antitissue transglutaminase antibodies was performed according to manufacturer's instructions (Elia Celikey, Phadia 250).

RESULTS AND DISCUSSION

Characterization of the Nanoelectrode Ensembles. Figure 1A shows FE-SEM images of the NEEs recorded before functionalization with the capture protein, tTG. One can clearly see the bright conductive Au nanoelectrodes surrounded by the insulating PC surface (black part). The pores of the template are filled by electroless deposition with Au-nanowires whose upper ends emerge on the surface of the template with the shape of nanodisks of approximately 50 nm diameter. The distance between the nanoelectrodes is rather variable, ranging between 100 and 400 nm. The density of nanoelectrodes measured from these images is 5×10^8 electrodes·cm^{-2}.

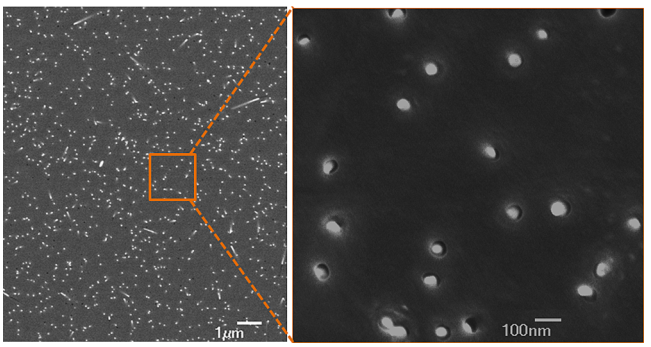

Figure 1. Field emission scanning electron microscopy (FE-SEM) images of a gold-NEE at two magnifications.

All these morphological data substantially match with those presented previously by Ugo et al.,[54] confirming that the diameter of the nanodisk electrodes is slightly higher than the diameter of the pores declared by the provider of the track-etched membrane (namely, 30 nm) with an electrode density substantially matching the declared pore density (5×10^8 vs 6×10^8, respectively).

ECL Detection Strategy Based on Immobilized Labels and Diffusing TPrA Radicals. In the present work, we report an original sensing strategy based on the spatial segregation between the electrochemical reaction and the biorecognition event. Considering the global ECL process, this means that the initial electron-transfer reactions occurring at the Au nanodisks are separated from the final step where light is emitted at the level of the nonconductive PC surface modified by the

biomolecules. Such a sensing approach does not require a direct electron transfer between the ECL label and the electrode surface and it is completely based on the so-called "revisited route".[37,39] In this mechanistic path, only the model coreactant TPrA is oxidized at the electrode, and the resulting radicals, $TPrA^{\bullet+}$ and $TPrA^{\bullet}$, play the central role in the ECL process:

$$TPrA - e \leftrightarrows TPrA^{\bullet+} \quad (1)$$

$$TPrA^{\bullet+} \leftrightarrows TPrA^{\bullet} + H^{+} \quad (2)$$

$$TPrA^{\bullet} + PC{-}\cdots{-}Ru(bpy)_3^{2+} \leftrightarrows Im^{+} + PC{-}\cdots{-}Ru(bpy)_3^{+} \quad (3)$$

$$TPrA^{\bullet+} + PC{-}\cdots{-}Ru(bpy)_3^{+} \leftrightarrows TPrA + PC{-}\cdots{-}Ru(bpy)_3^{2+*} \quad (4)$$

$$PC{-}\cdots{-}Ru(bpy)_3^{2+*} \rightarrow PC{-}\cdots{-}Ru(bpy)_3^{2+} + h\nu_{ECL} \quad (5)$$

where Im^{+} is the iminium product and $PC{-}\cdots{-}Ru(bpy)_3^{2+}$ represents the ruthenium label attached to the PC surface via the biorecognition chain described in Scheme 1.

The radical cation $TPrA^{\bullet+}$ is formed at the surface of the Au nanodisks by TPrA oxidation (reaction 1). While diffusing, it can undergo deprotonation to produce the strong reducing radical $TPrA^{\bullet}$ (reaction 2), which reduces the immobilized $Ru(bpy)_3^{2+}$ to $Ru(bpy)_3^{+}$ (reaction 3). This process is followed by the one-electron oxidation of $Ru(bpy)_3^{+}$ by the $TPrA^{\bullet+}$ radical cation to generate the excited state $Ru(bpy)_3^{2+}*$ on PC (reaction 4). Finally, $Ru(bpy)_3^{2+}*$ relaxes to the ground state by photon (ECL) emission (reaction 5).[34,56,57] It is worth mentioning that the factors which affect the lifetime of the radical cation, such as the pH,[58,59] should be critically controlled to ensure optimum proportion of $TPrA^{\bullet+}$ and $TPrA^{\bullet}$ at the site of emission. Indeed, the unstable nature of the radical cation is one of the factors that determines the maximum distance from the electrode at which ECL emission can occur. In alkaline solutions, deprotonation of $TPrA^{\bullet+}$ is enhanced, resulting in shortage of the cation at the site of emission. Based on the 0.2 ms half-life of the radical cation reported in the literature,[39] it can diffuse up to 3 μm from the site of formation,[37,39] which is a distance largely exceeding the maximum half-distance between the nanoelectrodes in our sensor (i.e., 200 nm). This means that both radicals generated by reactions 1 and 2 can live long enough to diffuse to the ruthenium label where reactions 3–5 take place on the PC surface (see Scheme 1).

ECL Immunoassay Platform. The ECL platform consists of an ensemble of nanoelectrodes delimited by an insulating PC film which is modified with a capture tTG protein. The assay was performed by incubating the modified NEEs first in a sample containing the target anti-tTG IgG antibody and then in a solution of a biotinylated detection antibody. Finally, the streptavidin-modified ECL label is attached to this secondary antibody on the PC surface. The $Ru(bpy)_3^{2+}$ label should bind only to the PC where the capture tTG protein is present and can be detected by performing a cyclic voltammogram in a PBS solution containing the TPrA coreactant. Figure 2A shows the voltammetric and ECL responses of the NEEs modified with the attached label in the presence of the coreactant. The anodic portion of the voltammetric curve is characterized by an oxidation peak at approximately 0.88 V versus Ag/AgCl, followed by a broad signal at about 1.2 V. In the backward scan, a cathodic peak is detected at about 0.25 V. The broad signal at 1.2 V is related to the formation of Au-oxides on the surface of

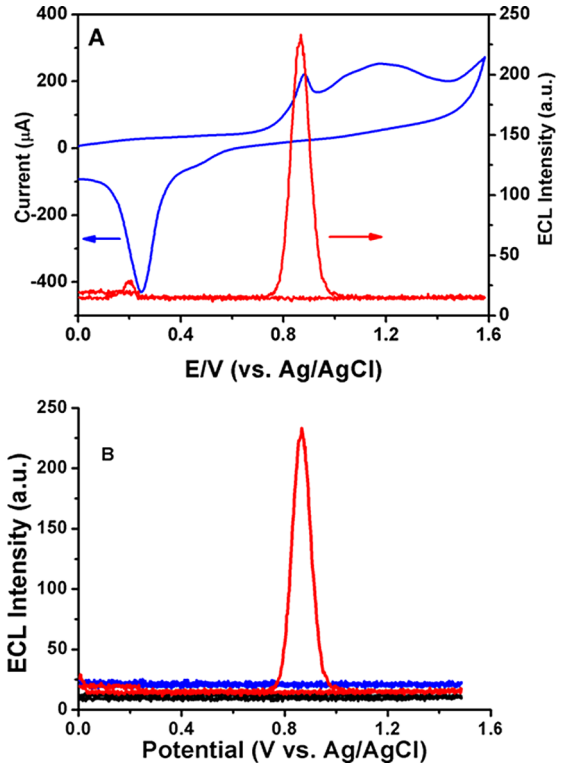

Figure 2. (A) Cyclic voltammogram (blue curve) and the corresponding ECL intensity (red curve) of the anti-tTG immunosensor obtained in a PBS solution (pH 7.4) containing 0.1 M TPrA. (B) ECL signals of bare NEEs (black curve) of the immunoassay recorded without (negative control - blue curve) and with (red curve) the incubation step in the presence of the anti-tTG antibody. Same solution as in panel A. Scan rate: 100 mV/s.

the nanoelectrodes, this oxide layer being reduced at 0.25 V in the backward scan. This agrees with previous literature findings[44] that demonstrate that the Au-oxides formation is anticipated at the nanoelectrodes with respect to bulk gold. The voltammetric peak at 0.88 V is attributed to the electrochemical oxidation of TPrA, as confirmed by differential pulse voltammetry (DPV) experiments (Figure S2 in Supporting Information). DPV was preferred to cyclic voltammetry for these measurements because it provides a better resolution to separate possibly overlapping peaks.

Data reported in Figure S2 indicate that a DPV peak at 0.88 V is clearly detected when a bare NEE is dipped in TPrA solution, and the peak amplitude increases with the TPrA concentration. The gray curve in Figure S1 was recorded by DPV in the presence of 100 μM $Ru(bpy)_3^{2+}$ but without TPrA and no peak corresponding to $Ru(bpy)_3^{2+}$ oxidation is visible up to 1 V versus Ag/AgCl. Finally, we recorded the DPV signal of the fully modified immunoassay platform in PBS, and we did not observe any peak corresponding to the oxidation of the ruthenium label. In addition, voltammetric experiments (Figure 2A) confirmed that the ruthenium complex is not oxidized on the Au nanodisks, even at the lower anodic potential (i.e., 0.88 V vs Ag/AgCl). As a whole, these results indicate that the ECL label is mainly immobilized on the PC surface.

When the immunosensor was incubated with the target antibody, a well-resolved ECL signal was recorded at 0.88 V versus Ag/AgCl (Figure 2). It is noteworthy that ECL is detected at the potential at which TPrA oxidation occurs, whereas no ECL signal is detected at the potential values

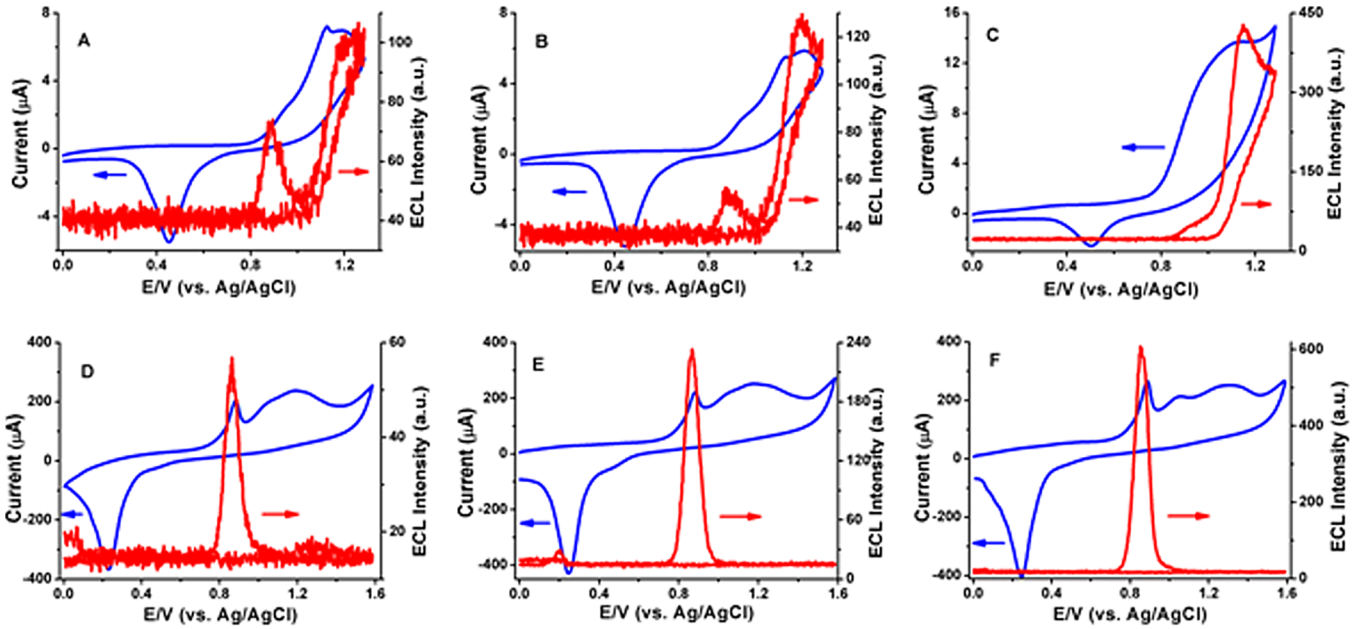

Figure 3. Effect of the amount of luminophore either dissolved in solution (curves A−C) or immobilized on PC (curves D−F) on the voltammetric (blue curves) and ECL responses (red curves) in 0.1 M PBS pH 7.4 solution containing 0.1 M TPrA. (A−C) Signals recorded at bare NEE after adding (A) 0.5, (B) 1.0, and (C) 10 μM $Ru(bpy)_3^{2+}$ in the solution. (D−F) Signals recorded with the immunosensor incubated with (D) 0.5, (E) 1, and (F) 10 $\mu g \cdot mL^{-1}$ anti-tTG protein.

usually expected for $Ru(bpy)_3^{2+}$ oxidation (namely, 1.2.V vs Ag/AgCl), even after repetitive scanning of the potential. This evidence that the direct oxidation of $Ru(bpy)_3^{2+}$ at the surface of the Au nanodisks is not occurring because the ruthenium label is specifically linked to the antibodies chain immobilized on the PC of the NEEs. Moreover, the central role of the TPrA oxidation in the present analytical strategy was also confirmed by comparing the voltammetric and ECL emission patterns observed when changing the $Ru(bpy)_3^{2+}$ concentration either when dissolved in solution (Figure 3A−C) or when bound onto the PC as a SA-$Ru(bpy)_3^{2+}$ label (Figure 3D−F). When $Ru(bpy)_3^{2+}$ is dissolved in solution (Figure 3A−C), two ECL peaks are recorded at around 0.9 and 1.2 V. Both ECL emission signals are better resolved with lower concentrations of ruthenium complex (e.g., 0.5 μM), while keeping constant the TPrA value to 0.1 M. Such a behavior was already reported in previous works,[39,60,61] and it agrees with the occurrence of two separated ECL emission processes: one related to TPrA oxidation at 0.9 V (i.e., the "revisited route") and the other to $Ru(bpy)_3^{2+}$ oxidation at 1.2 V[39] (namely the "catalytic route"). It is worth stressing that the intensity of the ECL emission at 1.2 V scales with the $Ru(bpy)_3^{2+}$ concentration. In the cyclic voltammograms in Figure 3A−C, the peak relevant to the formation of Au oxides on the surface of the NEEs, is located just before the $Ru(bpy)_3^{2+}$ oxidation peak, whereas the reduction of these oxides (backward scan) is detected at about 0.45 V. However, in Figure 3D−F (immunosensor), this peak is detected at 0.25 V. Such a difference is related to the different anodic limit adopted for the scans of Figure 3A−C and Figure 3D−F, namely, 1.25 V versus 1.6 V, respectively. Such a higher limit corresponds indeed to the formation of a more compact layer of Au-oxides, which is more difficult to reduce.

In the case of the immunoassay (Figure 3D−F), the amount of ECL label bound on the PC surface was tuned by changing the concentration of anti-tTG in the incubation solution. Higher anti-tTG concentrations favor more bounded secondary antibody and, consequently, more SA- $Ru(bpy)_3^{2+}$ finally attached on the PC. In this case, only one ECL emission peak is detected at 0.88 V, its maximum intensity depending on the amount of anti-tTG (i.e., $Ru(bpy)_3^{2+}$ label). As expected, the voltammetric signals remain practically unchanged from Figure 3D−F because TPrA oxidation and Au-oxides formation occur whatever the amount of label immobilized on the PC. Only for the highly amplified ECL signals in Figure 3D was a very small ECL emission detected in proximity of the $Ru(bpy)_3^{2+}$ oxidation potential (1.28 V), with an ECL peak emission that is not higher than 1% of the peak at 0.88 V. This confirms the negligible effect of nonspecific adsorption of eventual traces of the luminophore on the Au nanoelectrode surfaces. Control experiments were performed with bare NEEs and also with the immunosensor incubated with the secondary antibody and the SA- $Ru(bpy)_3^{2+}$ complex but in the absence of the monoclonal mouse anti-tTG antibody (Figure 2B). ECL intensity comparable to the background level is recorded in the former case. Moreover, in the later situation, the lack of ECL signal with this negative control indicates the absence of any nonspecific binding of the secondary antibody and/or SA-$Ru(bpy)_3^{2+}$ label. Both experiments confirm that when the anti-tTG target is absent, no $Ru(bpy)_3^{2+}$ label is bound onto the NEEs and no ECL is generated. Eventually, the fact that ECL emission occurs at an applied potential of 0.88 V, instead of 1.2 V as in usual ECL assays, leads to several analytical advantages. First, it significantly reduces possible interferences from side reactions while dealing with complex samples containing oxidizable species. Next, it may reduce the ECL background arising from the reaction between $Ru(bpy)_3^{3+}$ and hydroxide in aqueous systems.[60] Third, concerning the applicability of such biosensors, it may minimize electrochemical damage on sensitive biomolecules and oligonucleotide sequences.[60] Finally, it reduces oxide layer formation on Au or Pt electrode surfaces.

Analytical Performance of the Immunosensor and Its Application to Human Sera Measurements. Because standard human anti-tTG is unavailable on the market, the performance of the developed ECL-based immunosensor was initially evaluated using serial dilutions of standard mouse anti-tTG IgG antibody. The ECL responses for concentrations ranging from 1 ng·mL^{-1} to 10 μg·mL^{-1} are shown in Figure 4.

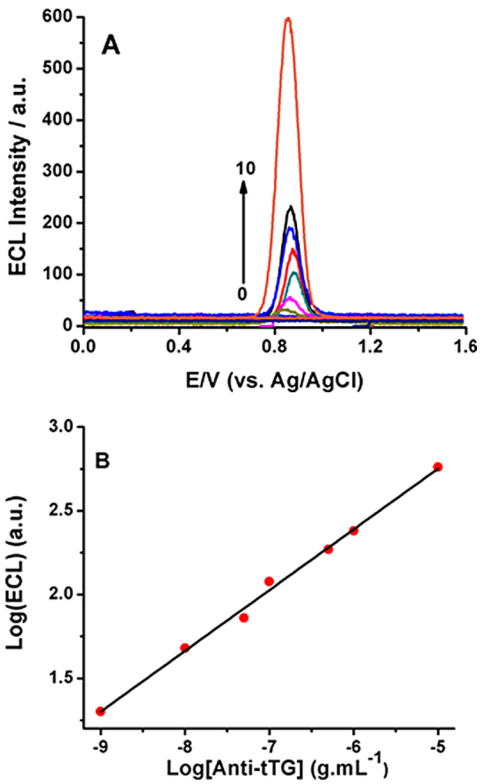

Figure 4. (A) Relationship between ECL intensity and the concentration of anti-tTG antibody. The arrow indicates increasing concentrations of this target antibody: 0.00, 0.001, 0.01, 0.05, 0.1, 0.5, 1, and 10 μg·mL^{-1}. (B) Log–log plot of ECL signal output as a function of the concentration of anti-tTG captured on the NEE platform (n = 3). Same experimental conditions as in Figure 2.

The relevant calibration plot in Figure 4B shows that the logarithm of the ECL peak intensity increases linearly with the logarithm of the anti-tTG concentration, (correlation coefficient R^2 = 0.995), over a wide dynamic range (10^{-9} – 10^{-5} g·mL^{-1} anti-tTG). A linear plot (with R^2 = 0.976) is also obtained for the direct dependence of the ECL intensity versus anti-tTG concentration, in the range 1–100 ng·mL^{-1} (Figure S4 in Supporting Information). Each analysis was performed with a different NEE which probably binds different amounts of proteins; a slight difference in the surface state of functionalized NEEs[62] could be the cause of the very slight shift (<20 mV) in the potential at which the maximum ECL emission is detected (see Figure 4A). Indeed, data in Figure 4B refer to the ECL intensity measured at the potential of maximum emission. Concerning the reproducibility of the ECL maximum intensity, we conducted measurements repeated on four different NEEs all incubated in 100 ng·mL^{-1} anti-tTG solutions, which provided a relative standard deviation of 3.4%, confirming a satisfactory precision. A limit of detection (LOD) of 0.47 ng·mL^{-1} was calculated by using the equation LOD = $3\sigma_b/m$,[63] where σ_b is the blank standard deviation (background noise) and m in the sensitivity (slope) of the linear calibration plot [ECL] intensity versus [anti-tTG].

The performances of the proposed immunosensor for the analysis of human serum samples were tested by determining anti-tTG level in seven human serum samples, diluted 1:200 with phosphate buffer. The secondary antibody used for these analyses is a biotinylated goat antihuman IgG antibody instead of the goat antimouse antibody used before to determine the mouse anti-tTG standard available on the market. For this reason, concentrations of anti-tTG IgG in the serum samples were not calculated as absolute values, but rather, they were evaluated comparatively with respect to standard fluoro-enzyme immunoassay (FEIA) determinations. The ECL emission curves, reported in Figure 5A, show well-resolved ECL peaks

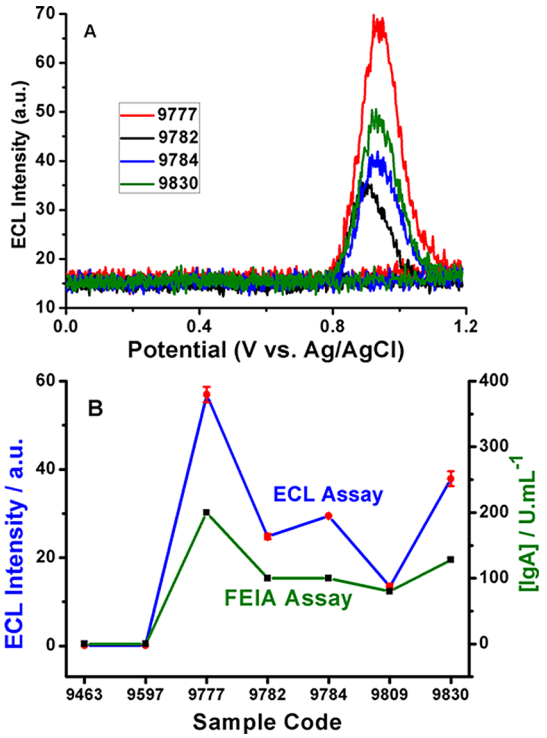

Figure 5. (A) ECL signals detected with immunosensors for the evaluation of anti-tTG level in human serum samples (diluted 1:200 in PBS); other experimental conditions as in Figure 2. (B) Comparison of ECL intensities measured by the proposed ECL immunoassay with clinical results determined by fluoro-enzyme immunoassay of serum samples from five CD patients (9777, 9782, 9784, 9809, 9830) and from two healthy individuals (9463, 9597).

for the four samples indicated in the inset, whereas two other samples produced ECL signals not distinguishable from the background noise (i.e., 9463 and 9597 samples). Note that for the positive samples, the recorded peaks appeared slightly larger in potential than the ECL peak obtained with the synthetic samples (see Figure 4), though this did not impair the analyses.

Results obtained with the ECL sensor were compared at first with data for anti-tTG, IgG class obtained by FEIA; however, all the FEIA data were below the cutoff value of the method (normal value <7 U·mL^{-1}). A different situation was observed when comparing ECL data with FEIA results for IgA anti-tTG. Data reported in Figure 5B shows a good agreement between the ECL and FEIA-IgA results. For the sake of readability, Figure 5A shows less data than Figure 5B. The two methods show parallel trends for both heathy subjects (samples 9463

and 9597) and for the celiac patients. Interestingly, the ECL results suggest a higher sensitivity to measure the IgG anti-tTG than the FEIA method, which identifies only IgA anti-tTG but not IgG anti-tTG antibodies.

CONCLUSIONS

This study demonstrates for the first time that nanoelectrode ensembles can be successfully used for the detection by ECL of target proteins, in particular the anti-tTG antibody used as biomarker for the serological diagnosis of the celiac disease. The composite nature of NEEs, made of Au nanodisk electrodes embedded in a polymeric template, allowed us to exploit the wide surface of the PC membrane to immobilize a capture agent (namely, the antigen tTG), the analyte and, finally, a luminescent ruthenium(II) label. According to this architecture, the nanoelectrodes act as electrochemical transducers for initiating the ECL emission while PC is exploited to perform the biorecogniton event and to bind the luminescent label. Consequently, the electrochemical initiation of the ECL emission results from the oxidation of the coreactant TPrA and not from that of the Ru(II) luminophore. Voltammetric and ECL data indicate indeed that the ruthenium complex is not oxidized directly at the surface of the nanoelectrodes, but instead, ECL is generated only by the electrochemical oxidation of TPrA, producing the radicals $TPrA^{\bullet+}$ and $TPrA^{\bullet}$ which live long enough to diffuse and to react with the luminophore, immobilized onto the neighboring PC membrane. Concerning the specific application goal, that is the serological diagnosis of the celiac disease, the NEE-based ECL sensors is characterized by high sensitivity, low detection limit, and wide dynamic range, and in addition, it can furnish diagnostically useful information for human serum analysis. The satisfactory agreement between data from the ECL sensor and from fluoro-enzyme immunoassays in different clinical samples support the extension of the study to a higher number of samples, in order to evaluate the clinical sensitivity and specificity of the method.

From an analytical point of view, a particular advantage of the sensor is that the ECL emission is obtained by applying a potential of 0.88 V versus Ag/AgCl, which is about 0.3 V lower than in the case when ECL is initiated by the electrochemical oxidation of $Ru(bpy)_3^{2+}$. The lower operative potential reduces significantly the possible interference from side reactions in samples containing oxidizable species. Moreover, it reduces the ECL background arising from the reaction between $Ru(bpy)_3^{3+}$ and hydroxide ions in aqueous samples. Finally, it minimizes possible electrochemical damage of sensitive biomolecules and oligonuceotide sequences, and it also reduces the oxide formation on Au or Pt electrode surfaces. These advantages can be extended to other ECL sensors by using the same NEE platform for the immobilization of other capture agents, potentially suitable for the biorecognition of a wide range of antigen or antibody or oligonucleotide targets.

ASSOCIATED CONTENT

Supporting Information:

Procedure and scheme to assemble the NEEs. Differential pulse voltammetric data recorded with a bare NEE in solution containing different concentrations of tri-*n*-propylamine or $Ru(bpy)_3^{2+}$. EDX microanalysis of the NEE surface. Dependence of ECL emission on the anti-tTG concentration in the 1−100 ng·mL^{-1} range (PDF)

AUTHOR INFORMATION

Corresponding Authors

*E-mail: sojic@enscbp.fr.

*E-mail: ugo@unive.it.

Notes

The authors declare no competing financial interest.

ACKNOWLEDGMENTS

This work was financially supported by MIUR (Rome), project PRIN 2010AXENJ8 and, partially, by the Cross-Border Cooperation Italy-Slovenia Program 2007−2013 − Strategic Project TRANS2CARE. H.B.H. is the grateful recipient of a mobility grant from the Erasmus Placement Program. M.S. acknowledges financial supports from the Ministry of Science and Technological Development (Republic of Serbia) and from the French Foreign Ministry (Bourse d'Excellence Eiffel).

REFERENCES

(1) Tommasini, A.; Not, T.; Kiren, V.; Baldas, V.; Santon, D.; Trevisiol, C.; Berti, I.; Neri, E.; Gerarduzzi, T.; Bruno, I.; Lenhardt, A.; Zamuner, E.; Spano, A.; Crovella, S.; Martellossi, S.; Torre, G.; Sblattero, D.; Marzari, R.; Bradbury, A.; Tamburlini, G.; Ventura, A. *Arch. Dis. Child.* **2004**, *89*, 512−515.

(2) Maki, M.; Mustalahti, K.; Kokkonen, J.; Kulmala, P.; Haapalahti, M.; Karttunen, T.; Ilonen, J.; Laurila, K.; Dahlbom, I.; Hansson, T.; Hopfl, P.; Knip, M. *N. Engl. J. Med.* **2003**, *348*, 2517−2524.

(3) Lohi, S.; Mustalahti, K.; Kaukinen, K.; Laurila, K.; Collin, P.; Rissanen, H.; Lohi, O.; Bravi, E.; Gasparin, M.; Reunanen, A.; Maki, M. *Aliment. Pharmacol. Ther.* **2007**, *26*, 1217−1225.

(4) Ventura, A.; Facchini, S. *Clin. Pediatr.* **2001**, *40*, 575−577.

(5) Hin, H.; Bird, G.; Fisher, P.; Mahy, N.; Jewell, D. *Br. Med. J.* **1999**, *318*, 164−167.

(6) Corrao, G.; Corazza, G. R.; Bagnardi, V.; Brusco, G.; Ciacci, C.; Cottone, M.; Guidetti, C. S.; Usai, P.; Cesari, P.; Pelli, M. A.; Loperfido, S.; Volta, U.; Calabro, A.; Certo, M. *Lancet* **2001**, *358*, 356−361.

(7) Hill, I. D. *Gastroenterology* **2005**, *128* (Suppl), S25−32.

(8) Korponay-Szabo, I. R.; Szabados, K.; Pusztai, J.; Uhrin, K.; Ludmány, E.; Nemes, E.; Kaukinen, K.; Kapitany, A.; Koskinen, L.; Sipka, S.; Imre, A.; Maki, M. *Br. Med. J.* **2007**, *335*, 1244−1247.

(9) Nemec, G.; Ventura, A.; Stefano, M.; Di Leo, G.; Baldas, V.; Tommasini, A.; Ferrara, F.; Taddio, A.; Città, A.; Sblattero, D.; Marzari, R.; Not, T. *Am. J. Gastroenterol.* **2006**, *101*, 1597−1600.

(10) Singh, P.; Wadhwa, N.; Chaturvedi, M. K.; Bhatia, V.; Saini, S.; Tandon, N.; Makharia, G. K.; Maki, M.; Not, T.; Phillips, A.; Bhatnagar, S. *Arch. Dis. Child.* **2014**, *99*, 1004−1008.

(11) Byass, P.; Kahn, K.; Ivarsson, A. *PLoS One* **2011**, *6*, e22774.

(12) Holding, S.; Wilson, F.; Spradbery, D. *J. Immunol. Methods* **2014**, *405*, 29−34.

(13) Lerner, A. *Int. J. Celiac Disease* **2014**, *2*, 64−66.

(14) Dahlbom, I.; Olsson, M.; Forooz, N. K.; Sjoholm, A. G.; Truedsson, L.; Hansson, T. *Clin. Diagn. Lab. Immunol.* **2005**, *12*, 254−258.

(15) Maglio, M.; Tosco, A.; Paparo, F.; Auricchio, R.; Granata, V.; Colicchio, B.; Indolfi, V.; Miele, E.; Troncone, R. *J. Pediatr. Gastroenterol. Nutr.* **2010**, *50*, 43−48.

(16) Wang, N.; Truedsson, L.; Elvin, K.; Andersson, B. A.; Ronnelid, J.; Mincheva-Nilsson, L.; Lindkvist, A.; Ludvigsson, J. F.; Hammarstrom, L.; Dahle, C. *PLoS One* **2014**, *9*, e93180.

(17) Scherf, K. A.; Koehler, P.; Wieser, H. *Adv. Chem. Eng. Sci.* **2015**, *5*, 83−95.

(18) Giannetto, M.; Mattarozzi, M.; Umiltà, E.; Manfredi, A.; Quaglia, S.; Careri, M. *Biosens. Bioelectron.* **2014**, *62*, 325−330.

(19) Kergaravat, S. V.; Beltramino, L.; Garnero, N.; Trotta, L.; Wagener, M.; Pividori, M. I.; Hernandez, S. R. *Biosens. Bioelectron.* **2013**, *48*, 203−209.
(20) Neves, M. M. P. S.; González-García, M. B.; Nouws, H. P. A.; Costa-García, A. *Biosens. Bioelectron.* **2012**, *31*, 95−100.
(21) Dulay, S.; Lozano-Sánchez, P.; Iwuoha, E.; Katakis, I.; O'Sullivan, C. K. *Biosens. Bioelectron.* **2011**, *26*, 3852−3856.
(22) Pividori, M. I.; Lermo, A.; Bonanni, A.; Alegret, S.; del Valle, M. *Anal. Biochem.* **2009**, *388*, 229−234.
(23) Liu, Z.; Qi, W.; Xu, G. *Chem. Soc. Rev.* **2015**, *44*, 3117−3142.
(24) Miao, W. *Chem. Rev.* **2008**, *108*, 2506−2553.
(25) Sardesai, N. P.; Barron, J. C.; Rusling, J. F. *Anal. Chem.* **2011**, *83*, 6698−6703.
(26) Hu, L.; Xu, G. *Chem. Soc. Rev.* **2010**, *39*, 3275−3304.
(27) Forster, R. J.; Bertoncello, P.; Keyes, T. E. *Annu. Rev. Anal. Chem.* **2009**, *2*, 359−385.
(28) Doeven, E. H.; Barbante, G. J.; Kerr, E.; Hogan, C. F.; Endler, J. A.; Francis, P. S. *Anal. Chem.* **2014**, *86*, 2727−2732.
(29) Chikkaveeraiah, B. V.; Bhirde, A. A.; Morgan, N. Y.; Eden, H. S.; Chen, X. *ACS Nano* **2012**, *6*, 6546−6561.
(30) Milutinovic, M.; Sallard, S.; Manojlovic, D.; Mano, N.; Sojic, N. *Bioelectrochemistry* **2011**, *82*, 63−68.
(31) Deiss, F.; LaFratta, C. N.; Symer, M.; Blicharz, T. M.; Sojic, N.; Walt, D. R. *J. Am. Chem. Soc.* **2009**, *131*, 6088−6089.
(32) Miao, W.; Bard, A. J. *Anal. Chem.* **2003**, *75*, 5825−5834.
(33) Blackburn, G. F.; Shah, H. P.; Kenten, J. H.; Leland, J.; Kamin, R. A.; Link, J.; Peterman, J.; Powell, M. J.; Shah, A.; Talley, D. B.; Tyagi, S. K.; Wilkins, E.; Wu, T.-J.; Massey, R. J. *Clin. Chem.* **1991**, *37*, 1534−1539.
(34) Muzyka, K. *Biosens. Bioelectron.* **2014**, *54*, 393−407.
(35) Sardesai, N.; Pan, S.; Rusling, J. *Chem. Commun.* **2009**, 4968−4970.
(36) Dominici, R.; Infusino, I.; Valente, C.; Moraschinelli, I.; Franzini, C. *Clin. Chem. Lab. Med.* **2004**, *42*, 945−951.
(37) Sentic, M.; Milutinovic, M.; Kanoufi, F.; Manojlovic, D.; Arbault, S.; Sojic, N. *Chem. Sci.* **2014**, *5*, 2568−2572.
(38) Miao, W.; Bard, A. J. *Anal. Chem.* **2004**, *76*, 7109−7113.
(39) Miao, W.; Choi, J. P.; Bard, A. J. *J. Am. Chem. Soc.* **2002**, *124*, 14478−14485.
(40) Menon, V. P.; Martin, C. R. *Anal. Chem.* **1995**, *67*, 1920−1928.
(41) Ugo, P.; Moretto, L. M.; Bellomi, S.; Menon, V. P.; Martin, C. R. *Anal. Chem.* **1996**, *68*, 4160−4165.
(42) Brunetti, B.; Ugo, P.; Moretto, L. M.; Martin, C. R. *J. Electroanal. Chem.* **2000**, *491*, 166−174.
(43) Pereira, F. C.; Moretto, L. M.; De Leo, M.; Zanoni, M. V. B.; Ugo, P. *Anal. Chim. Acta* **2006**, *575*, 16−24.
(44) Hulteen, J. C.; Menon, V. P.; Martin, C. R. *J. Chem. Soc., Faraday Trans.* **1996**, *92*, 4029−4032.
(45) Moretto, L. M.; Tormen, M.; De Leo, M.; Carpentiero, A.; Ugo, P. *Nanotechnology* **2011**, *22*, 185305−185311.
(46) Ugo, P.; Moretto, L. M.; De Leo, M.; Doherty, A. P.; Vallese, C.; Pentlavalli, S. *Electrochim. Acta* **2010**, *55*, 2865−2872.
(47) Ugo, P.; Moretto, L. M. In *Handbook of Electrochemistry*; Zoski, C., Ed.; Elsevier: Amsterdam, 2007; pp 678−709.
(48) Ongaro, M.; Ugo, P. *Anal. Bioanal. Chem.* **2013**, *405*, 3715−3729.
(49) Pozzi Mucelli, S.; Zamuner, M.; Tormen, M.; Stanta, G.; Ugo, P. *Biosens. Bioelectron.* **2008**, *23*, 1900−1903.
(50) Silvestrini, M.; Fruk, L.; Ugo, P. *Biosens. Bioelectron.* **2013**, *40*, 265−270.
(51) Silvestrini, M.; Ugo, P. *Anal. Bioanal. Chem.* **2013**, *405*, 995−1005.
(52) Bottari, F.; Oliveri, P.; Ugo, P. *Biosens. Bioelectron.* **2014**, *52*, 403−410.
(53) Habtamu, H. B.; Ugo, P. *Electroanalysis* **2015**, *27*, 2187−2193.
(54) Ugo, P.; Pepe, N.; Moretto, L. M.; Battagliarin, M. *J. Electroanal. Chem.* **2003**, *560*, 51−58.
(55) De Leo, M.; Pereira, F. C.; Moretto, L. M.; Scopece, P.; Polizzi, S.; Ugo, P. *Chem. Mater.* **2007**, *19*, 5955−5964.
(56) Zamolo, V. A.; Valenti, G.; Venturelli, E.; Chaloin, O.; Marcaccio, M.; Boscolo, S.; Castagnola, V.; Sosa, S.; Berti, F.; Fontanive, G.; Poli, M.; Tubaro, A.; Bianco, A.; Paolucci, F.; Prato, M. *ACS Nano* **2012**, *6*, 7989−7997.
(57) Chen, Z.; Zu, Y. *J. Phys. Chem. C* **2009**, *113*, 21877−21882.
(58) Wightman, R. M.; Forry, S. P.; Maus, R.; Badocco, D.; Pastore, P. *J. Phys. Chem. B* **2004**, *108*, 19119−19125.
(59) Moretto, L. M.; Kohls, T.; Badocco, D.; Pastore, P.; Sojic, N.; Ugo, P. *J. Electroanal. Chem.* **2010**, *640*, 35−41.
(60) Li, M.-J.; Chen, Z.; Yam, V.W.-W.; Zu, Y. *ACS Nano* **2008**, *2*, 905−912.
(61) Li, F.; Zu, Y. *Anal. Chem.* **2004**, *76*, 1768−1772.
(62) Silvestrini, M.; Schiavuta, P.; Scopece, P.; Pecchielan, G.; Moretto, L. M.; Ugo, P. *Electrochim. Acta* **2011**, *56*, 7718−7724.
(63) Long, G. L.; Winefordner, J. D. *Anal. Chem.* **1983**, *55*, 712A−724A.